Sliding-Mode Robot Control With Exponential Reaching Law

Charles J. Fallaha, Maarouf Saad, *Senior Member, IEEE*, Hadi Youssef Kanaan, *Senior Member, IEEE*, and Kamal Al-Haddad, *Fellow, IEEE*

***Abstract*—In this paper, sliding-mode control is applied on multi-input/multi-output (MIMO) nonlinear systems. A novel approach is proposed, which allows chattering reduction on control input while keeping high tracking performance of the controller in steady-state regime. This approach consists of designing a nonlinear reaching law by using an exponential function that dynamically adapts to the variations of the controlled system. Experimental study was focused on a MIMO modular robot arm. Experimental results are presented to show the effectiveness of the proposed approach, regarding particularly the chattering reduction on control input in steady-state regime.**

***Index Terms*—Chattering, control, exponential reaching law (ERL), modular robot, multi-input/multi-output (MIMO), nonlinear, sliding mode.**

I. Introduction

MANY NONLINEAR control techniques can be found in literature; among them, we find feedback linearization [1], fuzzy feedback linearization [2], backstepping [3]; [4], forwarding control [5] or adaptive backstepping [6], and sliding-mode control [7], which belongs to the family of variable structure controllers (VSCs) [8]. Sliding-mode control is based on the design of a high-speed switching control law that drives the system's trajectory onto a user-chosen hyperplane in the state space, also known as sliding surface. Sliding-mode control is an interesting approach, owing to its robustness and the simplicity of the derived control law. The key idea of the sliding-mode theory is to bring the study of an nth-order system to that of a first-order one by considering only the sliding function and its derivative as the new state variables.

The robustness of sliding-mode control can theoretically ensure perfect tracking performance despite parameters or model uncertainties. Thus, as far as robustness is concerned, sliding-mode control is ahead of other nonlinear techniques. In [9], the performance of a sliding-mode controller is studied using a hybrid controller applied to induction motors via sampled closed representations. The results were very conclusive regarding the effectiveness of the sliding-mode approach. An application of fuzzy sliding-mode control applied to 2 DOF can be found in [10], and in [11], the fuzzy sliding-mode approach is applied to a six-phase induction machine. A neuro-fuzzy sliding mode applied to induction machine can also be found in [12]. Finally, a neural-network sliding-mode approach is proposed in [13] to control a robot manipulator. In this particular case, the nonlinear dynamics of the robot is approximated using a radial basis function neural network. The backstepping technique [3], [14] is also a well-known nonlinear control approach based on the progressive construction of Lyapunov functions. However, backstepping control can only be applied to special classes of systems with a triangular dynamics structure, while sliding-mode control can be applied to a more general class of nonlinear systems and has the ability to consider robustness issues for modeling uncertainties and disturbances. In addition, the ability to specify performance directly makes sliding-mode control attractive from the design perspective.

Nonetheless, this approach is not flawless; indeed, in real-time applications, the switching control law in sliding mode is not instantaneous, and the sliding surface is not rigorously known. This leads to a high control activity, known as chattering. In most systems, the chattering phenomenon is undesirable because it can excite high-frequency dynamics which could be the cause of severe damage. Thus, many alternatives have been proposed to overcome this phenomenon. Floquet *et al.* [15] proposed a higher order sliding-mode control to reduce the chattering. This approach was also applied to trajectory tracking of robot by Hamerlain *et al.* [16]. Bartolini *et al.* [17], [18] proposed a second-order sliding-mode control in order to eliminate the discontinuous term in the control input (also treated in [19]). Moura and Olgac [20] proposed a VSC with a non-sliding regime, thus eliminating high-frequency oscillations. Camacho *et al.* [21] used a tuned sigmoid function instead of the *sign* function in order to reduce chattering effects.

An interesting approach in literature for chattering reduction is to change the reaching law by making the discontinuous gain k a function of S. Gao and Hung [22] based their study on this approach to reduce or even eliminate chattering on control input. One of the reaching laws they studied is based on power rate reaching strategy and uses the following reaching law:

$$\dot{S} = -k \cdot |S|^{\alpha} \mathrm{sign}(S), \qquad 0 \leq \alpha < 1. \tag{1}$$

Manuscript received April 14, 2009; revised August 14, 2009 and November 19, 2009; accepted February 25, 2010. Date of publication March 22, 2010; date of current version January 12, 2011. This work was supported in part by the Natural Sciences and Engineering Research Council of Canada under Grant 301160.

C. J. Fallaha, M. Saad, and K. Al-Haddad are with the Department of Electrical Engineering, École de Technologie Supérieure, Montreal, QC H3C 1K3, Canada (e-mail: charles.fallaha@etsmtl.ca; maarouf.saad@etsmtl.ca; kamal.al-haddad@etsmtl.ca).

H. Y. Kanaan is with the Department of Electrical and Mechanical Engineering, Faculty of Engineering, École Supérieure d'Ingénieurs of Beirut, Saint-Joseph University, Beirut 1107 2050, Lebanon (e-mail: hadi.kanaan@usj.edu.lb).

Color versions of one or more of the figures in this paper are available online at http://ieeexplore.ieee.org.

Digital Object Identifier 10.1109/TIE.2010.2045995

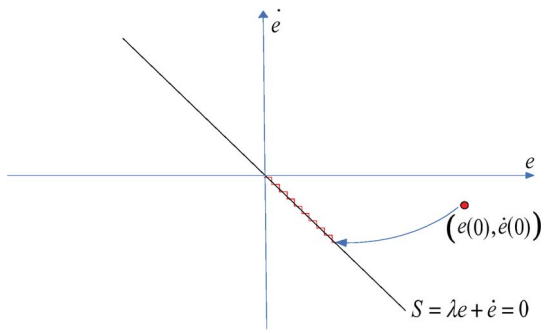

Fig. 1. Sliding-mode mechanism in phase plane.

However, in the aforementioned reaching law, the term $|S|^{\alpha}$ rapidly decreases because of the fractional power α, thus reducing the robustness of the controller near the sliding surface and also increasing the reaching time.

In order to propose a solution to the aforementioned problems, this paper introduces a new reaching law containing an exponential term functions of the sliding surface S. This reaching law is able to deal with the chattering/tracking performance dilemma. The exponential term smoothly adapts to the variations of S.

The rest of this paper is organized as follows. Section II exposes the problem formulation and motivation. The proposed exponential reaching law (ERL) is introduced in Section III. Section IV gives a general guideline for choosing ERL parameters for a system with uncertainties. Section V generalizes sliding-mode control to multi-input/multi-output (MIMO) systems. In Section VI, the new approach is tested experimentally on a robot arm, and real-time results are compared to the conventional sliding-mode approach. Section VII finally concludes the paper.

II. Problem Formulation and Motivation

A complete study of sliding-mode theory can be found in [3]. In this section, we briefly present its basic theory in which we emphasize on the most important advantages and its major drawbacks. These limitations motivate our research for a new reaching law approach that will be introduced in the next section. To explain sliding-mode approach, we consider the following second-order nonlinear system:

$$\ddot{x} = f(x, \dot{x}) + b(x, \dot{x}) \cdot u \tag{2}$$

where f and b are both nonlinear functions in terms of x and $\dot{x}$, and b is invertible. Let x_d be the reference trajectory and $e = x - x_d$ the tracking error which converges to zero. The first step in sliding-mode control is to choose the switching function S in terms of the tracking error. The typical choice of S in this particular case is

$$S = \lambda e + \dot{e}. \tag{3}$$

When the sliding surface is reached, the tracking error converges to zero as long as the error vector stays on the surface. The convergence rate is in direct relation with the value of λ. Fig. 1 shows how this mechanism takes place in the phase plane. From Fig. 1, it can be seen that there are two "modes" in the sliding-mode approach. The first mode, called reaching mode, is the step in which the error vector $(e, \dot{e})$ is attracted to the switching surface $S = 0$. In the second mode, also known as sliding mode, the error vector "slides" on the surface until it reaches the equilibrium point (0, 0).

Having chosen the sliding surface at this stage, the next step would be to choose the control law u that will allow error vector $(e, \dot{e})$ to reach the sliding surface. To do so, the control law should be designed in such a way that the following condition, also named reaching condition, is met:

$$S \cdot \dot{S} < 0 \qquad \forall t. \tag{4}$$

In order to satisfy condition (4), $\dot{S}$ is typically chosen as follows:

$$\dot{S} = -k \cdot \text{sign}(S) \qquad \forall t,\ k > 0. \tag{5}$$

Expression (5) is also called reaching law. Integrating (5) with respect to time yields the reaching time t_r, which is the required time for error vector $(e, \dot{e})$ to reach S

$$t_r = \frac{|S(0)|}{k}. \tag{6}$$

One can see from (6) that the reaching speed is increased with high values of k.

Taking into account the previous conditions, it is easy to show that the control input u has the following form [23]:

$$u = u_{\text{eq}} + u_{\text{disc}} \tag{7}$$

where

$$\begin{aligned} u_{\text{eq}} &= b^{-1}(\ddot{x}_d - \lambda \dot{e} - f) \\ u_{\text{disc}} &= -b^{-1} k \cdot \text{sign}(S). \end{aligned} \tag{8}$$

This control law shows that the control input contains the discontinuous term $b^{-1}k \cdot \text{sign}(S)$. This leads to the phenomenon of chattering. One can see that the chattering level is directly controlled by k. Therefore, the following dilemma arises: *In order to have a faster reaching time, a good robustness and tracking performance kmust be increased; however, this will directly increase the chattering level on the control input*. In order to solve this dilemma, the interdependence between the reaching time and the chattering level should be removed. The ERL, presented in the next section, is designed to solve this problem.

III. Sliding Mode With ERL

The reaching law proposed in this paper is based on the choice of an exponential term that adapts to the variations of the switching function. This reaching law is given by

$$\dot{S} = -\frac{k}{N(S)} \cdot \text{sign}(S), \qquad k > 0 \tag{9}$$

where

$$N(S) = \delta_0 + (1 - \delta_0) e^{-\alpha |S|^p}. \tag{10}$$

δ_0 is a strictly positive offset that is less than one, p is a strictly positive integer, and α is also strictly positive. Note that the ERL given by (9) does not affect the stability of the control because $N(S)$ is always strictly positive. From the reaching law stated in (9), one can see that if $|S|$ increases, $N(S)$ approaches δ_0, and therefore, $k/N(S)$ converges to k/δ_0, which is greater than k. This means that $k/N(S)$ increases in reaching phase, and consequently, the attraction of the sliding surface will be faster. On the other hand, if $|S|$ decreases, then $N(S)$ approaches one, and $k/N(S)$ converges to k. This means that, when the system approaches the sliding surface, $k/N(S)$ gradually decreases in order to limit the chattering. Therefore, the ERL allows the controller to dynamically adapt to the variations of the switching function by letting $k/N(S)$ to vary between k and k/δ_0.

Remark: If δ_0 is chosen to be equal to one, the reaching law of (9) becomes identical to that of (5). Therefore, the conventional reaching law becomes a particular case of the proposed approach.

Proposition 1: For the same gain k, the ERL given by (9) ensures a reaching time always smaller than that of the conventional reaching law expressed in (5).

Proof: Let t'_r be the reaching time for (9). Using the same relation, one has

$$\dot{S}\left[\delta_0 + (1-\delta_0)e^{-\alpha|S|^p}\right] = -k \cdot \text{sign}(S). \tag{11}$$

Integrating (11) between zero and t'_r and noticing that $S(t'_r)=0$ yield

$$t'_r = \frac{1}{k}\left(\delta_0 \left|S(0)\right| + (1-\delta_0)\int_0^{S(0)} \text{sign}(S)e^{-\alpha|S|^p}\cdot dS\right). \tag{12}$$

If $S \le 0$ for $t \le t'_r$, then

$$\int_0^{S(0)} \text{sign}(S)e^{-\alpha|S|^p}\,dS = -\int_0^{S(0)} e^{-\alpha|S|^p}\,dS = \int_0^{-S(0)} e^{-\alpha|S|^p}dS. \tag{13}$$

On the other hand, if $S \ge 0$ for $t \le t'_r$, then

$$\int_0^{S(0)} \text{sign}(S)e^{-\alpha|S|^p}\,dS = \int_0^{S(0)} e^{-\alpha|S|^p}\,dS. \tag{14}$$

Therefore, one can combine the last two expressions into the following:

$$\int_0^{S(0)} \text{sign}(S)e^{-\alpha|S|^p}\,dS = \int_0^{|S(0)|} e^{-\alpha|S|^p}\,dS. \tag{15}$$

Thus, the expression of t'_r given by (12) can be rewritten as follows:

$$t'_r = \frac{1}{k}\left(\delta_0 \left|S(0)\right| + (1-\delta_0)\int_0^{|S(0)|} e^{-\alpha|S|^p}\,dS\right). \tag{16}$$

Now, subtracting (6) from (16) yields

$$t'_r - t_r = \frac{1}{k}\left(-(1-\delta_0)|S(0)| + (1-\delta_0)\int_0^{|S(0)|} e^{-\alpha|S|^p}\,dS\right) \tag{17}$$

which can also be written as

$$t'_r - t_r = \frac{(1-\delta_0)}{k}\left(\int_0^{|S(0)|}\left[e^{-\alpha|S|^p} - 1\right]\,dS\right). \tag{18}$$

However, the term $e^{-\alpha|S|^p} - 1$ is always negative, which implies that $t'_r - t_r \le 0$.

For the particular case of $p = 1$, the expression of t'_r can be given by an analytical form. Indeed, considering (16) for $p = 1$ yields

$$t'_r = \frac{1}{k}\left(\delta_0 \left|S(0)\right| + \frac{(1-\delta_0)}{\alpha}\left[1 - e^{-\alpha|S(0)|}\right]\right). \tag{19}$$

Proposition 1: Shows that ERL increases the reaching speed of the sliding function while keeping the same gain k (i.e., the same chattering level). Also, for the same reaching time, the gain k needed for the reaching law of (9) is smaller than the k needed for (5). Therefore, for the same reaching speed, the proposed approach reduces chattering, which is a substantial asset over the conventional sliding-mode control.

IV. Choice of ERL Parameters

This section gives a general idea about the role of ERL parameters and the way they can be chosen in the control design. It is shown how system uncertainties can affect the choice of ERL parameters to maintain the robustness of the controller. A similarity with the boundary layer approach is also observed.

A. System Without Parameter Uncertainties

In the case where the system has no parameter uncertainties, the most important factor for choosing ERL parameters is the desired reaching time t_{rd}. From (16), it can be shown (proof is in the Appendix) that the reaching time t'_r for ERL approach verifies

$$t'_r \le \frac{\delta_0}{k}\left|S(0)\right| + \frac{(1-\delta_0)}{k\alpha^{1/p}}. \tag{20}$$

Therefore, if we choose

$$\frac{\delta_0}{k}\left|S(0)\right| + \frac{(1-\delta_0)}{k\alpha^{1/p}} = t_{rd} \tag{21}$$

we can guarantee that the reaching time t_r' is less than the desired reaching time t_{rd}. Moreover, if we choose α such that

$$\alpha \gg \left(\frac{1-\delta_0}{\delta_0\,|S(0)|}\right)^{1/p} \tag{22}$$

(21) can be rewritten as follows:

$$k \approx \delta_0 \frac{|S(0)|}{t_{rd}} \tag{23}$$

whereas in the conventional sliding-mode control

$$k = \frac{|S(0)|}{t_{rd}}. \tag{24}$$

Therefore, gain k can be tuned to a desired value with δ_0. Thus, without any parameter uncertainty, the choice of the ERL parameters is only bound by relations (22) and (23).

B. System With Bounded Uncertainties

Considering now a system with bounded uncertainties will obviously add more constraints in choosing ERL parameters. For simplification purposes, consider system (2) with $b(x,\dot{x}) = 1$

$$\ddot{x} = f(x,\dot{x}) + u \tag{25}$$

where $f(x,\dot{x})$ includes modeling uncertainties. Let $\hat{f}(x,\dot{x})$ be the estimate of $f(x,\dot{x})$ and L_{MAX} be the superior bound of the error between f and $\hat{f}$

$$L_{\mathrm{MAX}} = \sup_t \left| f(x,\dot{x}) - \hat{f}(x,\dot{x}) \right|. \tag{26}$$

With the same sliding function chosen as in (3), the conventional sliding-mode control law is given by

$$u(t) = -\lambda(\dot{x} - \dot{x}_d) + \ddot{x}_d - \hat{f}(x,\dot{x}) - k \cdot \mathrm{sign}(S). \tag{27}$$

This yields

$$\dot{S} = \left(f(x,\dot{x}) - \hat{f}(x,\dot{x})\right) - k \cdot \mathrm{sign}(S). \tag{28}$$

According to (28), in order for the sliding function to converge to zero, gain k must verify

$$k > \left| f(x,\dot{x}) - \hat{f}(x,\dot{x}) \right| \qquad \forall\, t. \tag{29}$$

Since k is a constant in conventional sliding mode, (29) implies that

$$k > L_{\mathrm{MAX}}. \tag{30}$$

Condition (30) is aggressive in the sense that gain k is overdimensioned to ensure the convergence of the sliding function.

With ERL approach, (30) can be written as

$$k > \delta_0 \cdot L_{\mathrm{MAX}} + (1-\delta_0) \cdot e^{-\alpha |S|^p} \cdot L_{\mathrm{MAX}}. \tag{31}$$

From (31), one can see that k has to be at least greater than $\delta_0 \cdot L_{\mathrm{MAX}}$. By choosing this minimum requirement for k and solving for S in (31) we have the following:

$$|S| > \sqrt[p]{\frac{\ln\left(\frac{L_{\mathrm{MAX}}(1-\delta_0)}{k-\delta_0 \cdot L_{\mathrm{MAX}}}\right)}{\alpha}}, \qquad k > \delta_0 \cdot L_{\mathrm{MAX}}. \tag{32}$$

Relation (32) shows that, in order to meet condition (31), sliding function S has to vary in a boundary of width W, given by

$$W = \sqrt[p]{\frac{\ln\left(\frac{L_{\mathrm{MAX}}(1-\delta_0)}{k-\delta_0 \cdot L_{\mathrm{MAX}}}\right)}{\alpha}}. \tag{33}$$

W is directly controlled with α.

At this stage, a similarity can be drawn between ERL and the conventional boundary layer approach that is widely discussed in scientific literature. Boundary layer approach consists of replacing discontinuous term $\mathrm{sign}(S)$ with $\mathrm{sat}(S/\phi)$

$$\mathrm{sat}(S/\phi) = \begin{cases} -1, & \text{for } S \le -\phi \\ S/\phi, & \text{for } -\phi \le S \le \phi \\ 1, & \text{for } S \ge \phi. \end{cases} \tag{34}$$

The boundary width for the sat function is given by

$$W = \frac{\phi \cdot L_{\mathrm{MAX}}}{k}, \qquad k > L_{\mathrm{MAX}}. \tag{35}$$

The width in this case is directly controlled by ϕ, similar to α. However, gain k has still to be larger than L_{MAX}, and the reaching time for the boundary layer approach is not finite. Hence, the superiority of ERL approach lies in the fact that it introduces independent and tunable parameters that meet the reaching time, the bounded-uncertainty condition, and the boundary layer width for the latter without having to overdimension gain k.

Combining the constraints in paragraphs A and B leads to the following relations which represent a general guideline on how ERL parameters can be chosen for the controller's design:

$$\frac{k}{\delta_0} > L_{\mathrm{MAX}} \qquad \alpha \ge \frac{\ln\left(\frac{L_{\mathrm{MAX}}(1-\delta_0)}{k-\delta_0 \cdot L_{\mathrm{MAX}}}\right)}{W^p}$$
$$\alpha \gg \left(\frac{1-\delta_0}{\delta_0\,|S(0)|}\right)^{1/p}. \tag{36}$$

Fig. 2 shows that, in order to keep the same reaching time t_r, the ERL can change the concavity of the switching function in terms of time by tuning the parameters k and δ_0. Note that if α is also chosen according to (22), then

$$\frac{k_1}{\delta_{01}} = \frac{k_2}{\delta_{02}} = \frac{k_3}{\delta_{03}} = k = \frac{|S(0)|}{t_r}, \qquad \text{with } \delta_{03} \le \delta_{02} \le \delta_{01}.$$

This means that, when δ_0 is decreased, gain k is decreased in the same proportion, yielding therefore less chattering in sliding

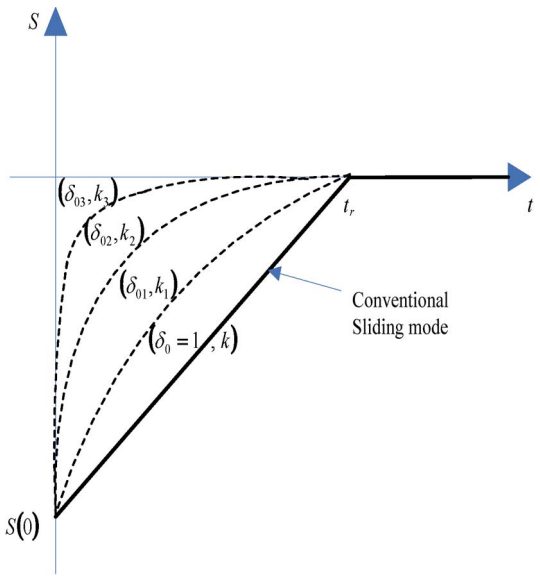

Fig. 2. Switching function with ERL for different values of k and δ_0.

mode. The decrease of gain k can be graphically interpreted by smaller slopes of the switching function when the sliding surface is reached. Note that the conventional reaching law is obtained for $\delta_0 = 1$.

V. Sliding-Mode Control for MIMO Systems

In this section, we extend the study of sliding-mode control to MIMO systems. We particularly focus on square systems of the form [23]

$$x_i^{(ni)} = f_i(X) + \sum_{j=1}^{m} b_{ij}(X)u_j, \qquad i = 1, \ldots, m. \tag{37}$$

The systems described by (37) are the said square systems, because the number of control inputs u_j is equal to that of the independent output variables x_i and can be expressed in the following matrix form:

$$X_n = \Phi(X) + \mathrm{B}(X) \cdot U \tag{38}$$

where $X_n = [\, x_1^{(n1)} \quad x_2^{(n2)} \quad \cdots \quad x_i^{(ni)} \quad \cdots \quad x_m^{(nm)} \,]^{\mathrm{T}}$; $\Phi = [\, f_1 \quad f_2 \quad \cdots \quad f_i \quad \cdots \quad f_m \,]^{\mathrm{T}}$; $B = [b_{ij}]$ with $i = 1, \ldots, m$ and $j = 1, \ldots, m$; $U = [\, u_1 \quad u_2 \quad \cdots \quad u_i \quad \cdots \quad u_m \,]^{\mathrm{T}}$; and X is defined as shown at the bottom of the page. Note that

$$\dim(X_n) = \dim(\Phi) = \dim(U) = (m \times 1)$$

$$\dim(\mathrm{X}) = \left(\left(\sum_{k=1}^{m} n_k \right) \times 1 \right).$$

Having m independent output variables to control in this case, we therefore need to design m independent sliding functions for each of the output variables. Let X_d be the desired reference vector defined as shown at the bottom of the page. Let also

$$E_i = \left[\underbrace{x_i - x_{di} \quad x_i^{(1)} - x_{di}^{(1)} \quad x_i^{(ni-1)} - x_{di}^{(ni-1)}}_{ni} \right]^{\mathrm{T}}$$

be the ith error vector corresponding to the ith independent variable x_i. We can build the m sliding functions as follows:

$$S_i = \Lambda_i^{\mathrm{T}} \cdot E_i, \qquad i = 1, \ldots, m \tag{39}$$

where $\Lambda_i = [\lambda_{1,i}, \lambda_{2,i}, \ldots, \lambda_{ni,i}]^{\mathrm{T}}$. Note that all Λ_i's have to be chosen such that the sliding surfaces $S_i = 0$ are stable differential equations that allow the error vectors to converge to zero. Let us compute $\dot{S}_i$ from (39)

$$\begin{aligned} \dot{S}_i &= \Lambda_i^T \cdot \dot{E}_i \\ &= \sum_{k=1}^{ni-1} \lambda_{k,i} \left(x_i^{(k)} - x_{di}^{(k)} \right) + \lambda_{ni,i} \cdot \left(x_i^{(ni)} - x_d^{(ni)} \right), \\ &\qquad i = 1, \ldots, m. \end{aligned} \tag{40}$$

Let $\nu_i = \sum_{k=1}^{ni-1} \lambda_{k,i}(x_i^{(k)} - x_{di}^{(k)}) - \lambda_{ni,i} \cdot x_d^{(ni)}$, and consider the following notations that apply for the rest of the development in this section:

$$\begin{aligned} \Sigma &= [\, S_1 \quad S_2 \quad \cdots \quad S_m \,]^{\mathrm{T}} \\ \dot{\Sigma} &= [\, \dot{S}_1 \quad \dot{S}_2 \quad \cdots \quad \dot{S}_m \,]^{\mathrm{T}} \\ \mathrm{sign}(\Sigma) &= [\, \mathrm{sign}(S_1) \quad \mathrm{sign}(S_2) \quad \cdots \quad \mathrm{sign}(S_m) \,]^{\mathrm{T}} \\ V &= [\, \nu_1 \quad \nu_2 \quad \cdots \quad \nu_m \,]^{\mathrm{T}} \\ \Gamma &= \mathrm{diag}(\lambda_{ni,i}, i = 1, \ldots m). \end{aligned}$$

$$X = \left[\underbrace{x_1 \quad x_1^{(1)} \quad x_1^{(n1-1)}}_{n1} \quad \underbrace{x_2 \quad x_2^{(1)} \quad x_2^{(n2-1)}}_{n2} \quad \cdots \quad \underbrace{x_i \quad x_i^{(1)} \quad x_i^{(ni-1)}}_{ni} \quad \cdots \quad \underbrace{x_m \quad x_m^{(1)} \quad x_m^{(nm-1)}}_{nm} \right]^T$$

$$X_d = \left[\underbrace{x_{d1} \quad x_{d1}^{(1)} \quad x_{d1}^{(n1-1)}}_{n1} \quad \underbrace{x_{d2} \quad x_{d2}^{(1)} \quad x_{d2}^{(n2-1)}}_{n2} \quad \cdots \quad \underbrace{x_{di} \quad x_{di}^{(1)} \quad x_{di}^{(ni-1)}}_{ni} \quad \cdots \quad \underbrace{x_{dm} \quad x_{dm}^{(1)} \quad x_{dm}^{(nm-1)}}_{nm} \right]^{\mathrm{T}}$$

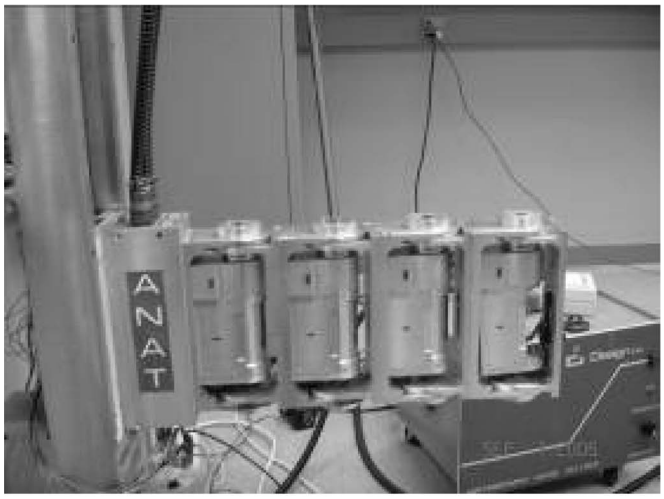

(a)

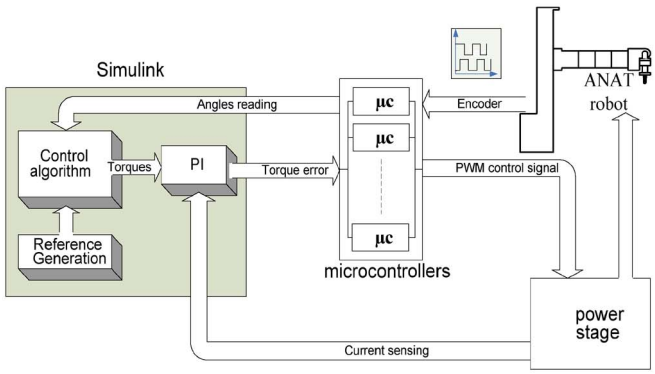

(b)

Fig. 3. Real-time setup. (a) ANAT robot arm. (b) Control scheme of the robot.

Equation (40) can therefore be written in the following matrix form:

$$\dot{\Sigma} = V + \Gamma \cdot X_n. \tag{41}$$

Finally, the following control law is obtained:

$$U = -(\Gamma \cdot B)^{-1}(V + \Gamma \cdot \Phi) - (\Gamma \cdot B)^{-1} K(\Sigma) \cdot \operatorname{sign}(\Sigma) \tag{42}$$

where

$$K(\Sigma) = \operatorname{diag}\left(\frac{k_i}{N_i(S_i)}, i = 1, \ldots, m\right)$$
$$N_i(S_i) = \delta_{0i} + (1 - \delta_{0i}) e^{-\alpha_i |S_i|^{pi}}.$$

Note that the matrix $(\Gamma \cdot B)$ is invertible only if B is a full rank.

VI. Case Study: ERL Sliding Mode Applied on Robotic Arm

As an application to sliding-mode control on MIMO systems, the robot arm ANAT shown in Fig. 3(a) is studied in this section with 3 DOF.

The real-time controller was implemented in Simulink with Real-Time Workshop (RTW) of Mathworks, Inc. The real-time target was chosen to be a National Instruments PCI 6024E digital card. Then, the control signals exiting from Simulink are applied to the ATMEGA 16 microcontrollers. Pulsewidth modulation equivalents are found and applied to the H-bridge drives of the three actuators of the robot arm. In order to complete the feedback loop, current sensors located in the H-bridge drives measure the current of each actuator and feed it back to Simulink for filtering and processing. Angular position loops are also fed to Simulink via the microcontrollers which process the digital information of the actuators' encoders. Fig. 3(b) shows the complete control scheme applied on the robot.

The dynamics of the robot are given by the well-known equation for rigid manipulators [24]

$$\ddot{q} = -M(q)^{-1} F(q, \dot{q}) + M(q)^{-1} \tau \tag{43}$$

where M is the inertia matrix, which is symmetric and positive definite. Thus, $M(q)^{-1}$ always exits. F is the centrifugal, Coriolis, and gravity vector; q is the joint position vector; and τ is the torque input vector of the manipulator. First, define a desired trajectory q_i^d, and define the tracking error for each joint as $e_i = q_i - q_i^d$, where $i = 1, 2, 3$.

Now, comparing (43) with (38) in Section IV gives the following equivalencies:

$$\ddot{q} \leftrightarrow X_n \qquad -M(q)^{-1} F(q, \dot{q}) \leftrightarrow \Phi(X)$$
$$M(q)^{-1} \leftrightarrow B(X) \qquad \tau \leftrightarrow U$$

and yields to the following control torques for the robot:

$$\tau = -M \cdot (\Lambda \dot{E} - \ddot{q}^d) + F - M \cdot K(\Sigma) \cdot \operatorname{sign}(\Sigma) \tag{44}$$

where $\Sigma = [\, S_1 \quad S_2 \quad S_3 \,]^{\mathrm{T}}$ is the sliding surface of the robot with $S_i = \lambda_i e_i + \dot{e}_i$, $i = 1, \ldots, 3$ the sliding surface of each DOF. $\Gamma = I_3$ in this case, and

$$K(\Sigma) = \operatorname{diag}\left(\frac{k_1}{N_1(S_1)}, \frac{k_2}{N_2(S_2)}, \frac{k_1}{N_2(S_2)}\right)$$
$$\dot{E} = [\, \dot{e}_1 \quad \dot{e}_2 \quad \dot{e}_3 \,]^{\mathrm{T}} \qquad \Lambda = \operatorname{diag}(\lambda_1, \lambda_2, \lambda_3)$$
$$\ddot{q}^d = [\, \ddot{q}_1^d \quad \ddot{q}_2^d \quad \ddot{q}_3^d \,]^{\mathrm{T}}.$$

The following experimental results are obtained with a smooth fifth-order polynomial reference trajectory:

$$\begin{aligned} q_i^d(t) = {} & a_{qi5}(t - t_{0i})^5 + a_{qi4}(t - t_{0i})^4 \\ & + a_{qi3}(t - t_{0i})^3 + a_{qi2}(t - t_{0i})^2 \\ & + a_{qi1}(t - t_{0i})^1 + a_{qi0}, \qquad i = 1, 2, 3 \end{aligned} \tag{45}$$

where

$$a_{qi5} = \frac{6\left(q_{if}^d - q_{i0}^d\right)}{t_1^5}$$
$$a_{qi4} = \frac{15\left(q_{if}^d - q_{i0}^d\right)}{t_1^4}$$
$$a_{qi3} = \frac{10\left(q_{if}^d - q_{i0}^d\right)}{t_1^3}$$

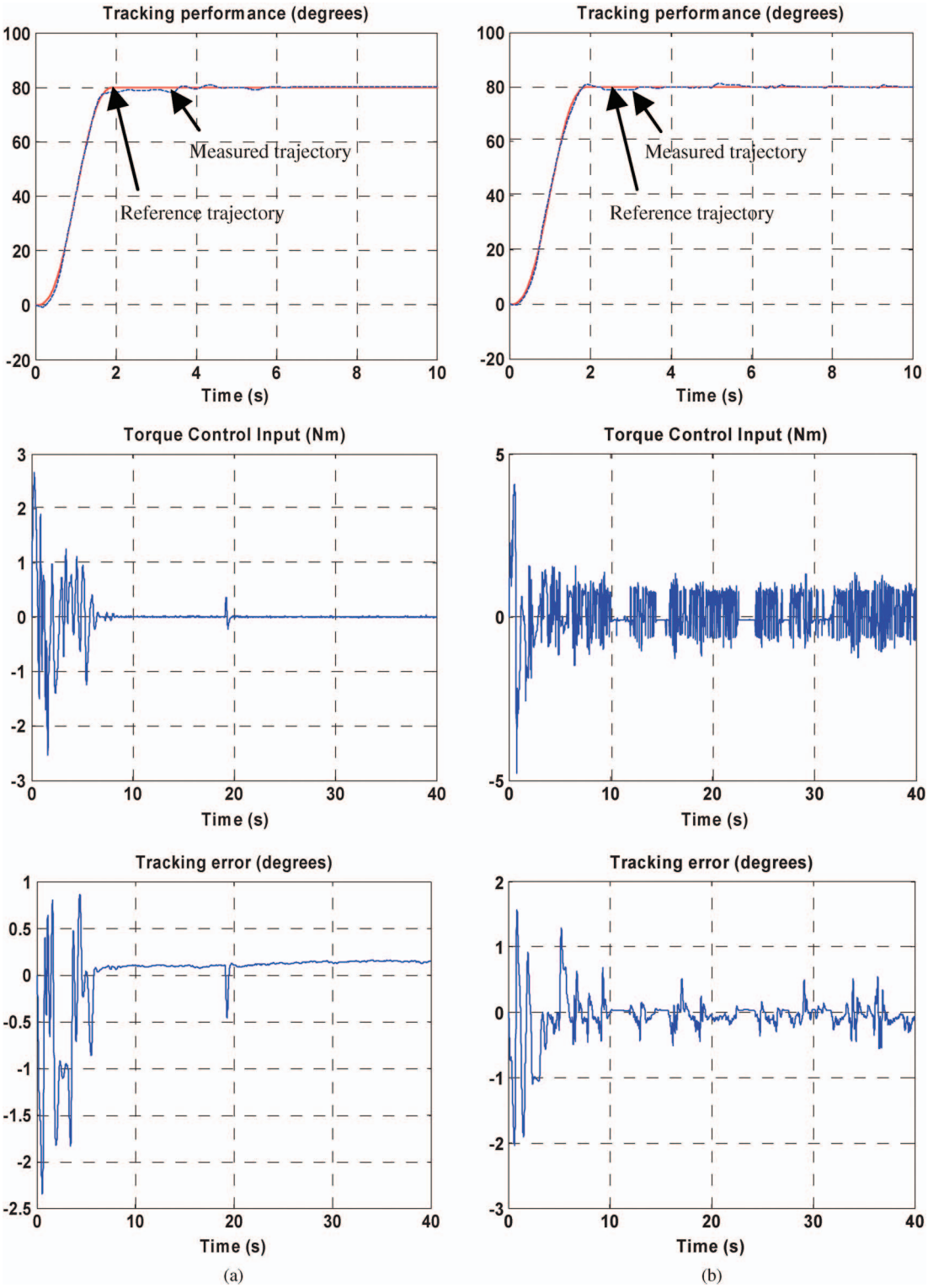

Fig. 4. Experimental results for joint 1 (a) with the reaching law and (b) with the conventional law. (a) ERL approach. (b) Conventional approach.

$a_{qi2} = a_{qi1} = 0$; $a_{qi0} = q_{i0}^d$; q_{i0}^d and q_{if}^d are the desired initial and final joint angles of link i, respectively; t_{0i} is the starting time of the reference trajectory for joint i; and t_1 is the time required for the reference trajectory to reach q_{if}^d, starting from q_{i0}^d.

The Appendix gives the values of the parameters for the reference trajectory and for all the other parameters of the controller. Note that, in order to test the robustness of the controller, the dynamical parameters of the robot arm are not measured but rather roughly estimated.

Figs. 4–6 show the experimental results for the three joints of ANAT arm. These figures compare the ERL approach, as shown in Figs. 4(a)–6(a), to that of the conventional sliding-mode approach, as shown in Figs. 4(b)–6(b). These results show the

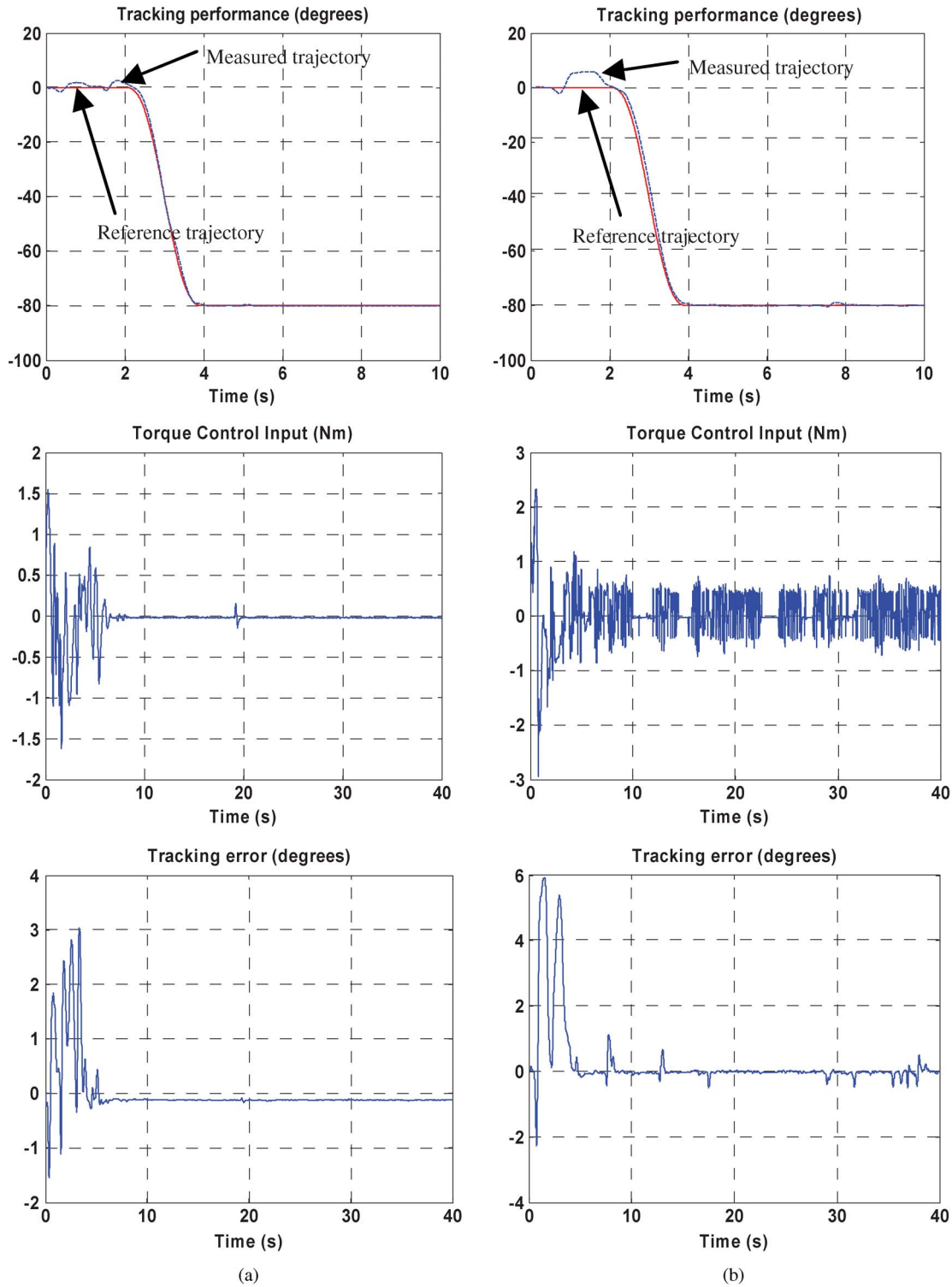

Fig. 5. Experimental results for joint 2 (a) with the reaching law and (b) with the conventional law. (a) ERL approach. (b) Conventional approach.

effectiveness of the proposed approach, regarding particularly the chattering reduction on the torque input. The steady-state error with ERL approach is due to the parameter uncertainties of the robot's model. However, it is bounded to be less than 0.1° for all three axes, and it can also be directly controlled by the value of α according to the condition given in (36). Therefore, with the ERL approach, the controller is able to reduce chattering on the control input while maintaining a very good tracking performance of the desired trajectory, although the reaching time remains the same. This is not possible to achieve with conventional sliding-mode approach. In the tracking performance figures (Figs. 4–6), the solid line represents the reference trajectory, and the dashed line represents the actual trajectory of the joint.

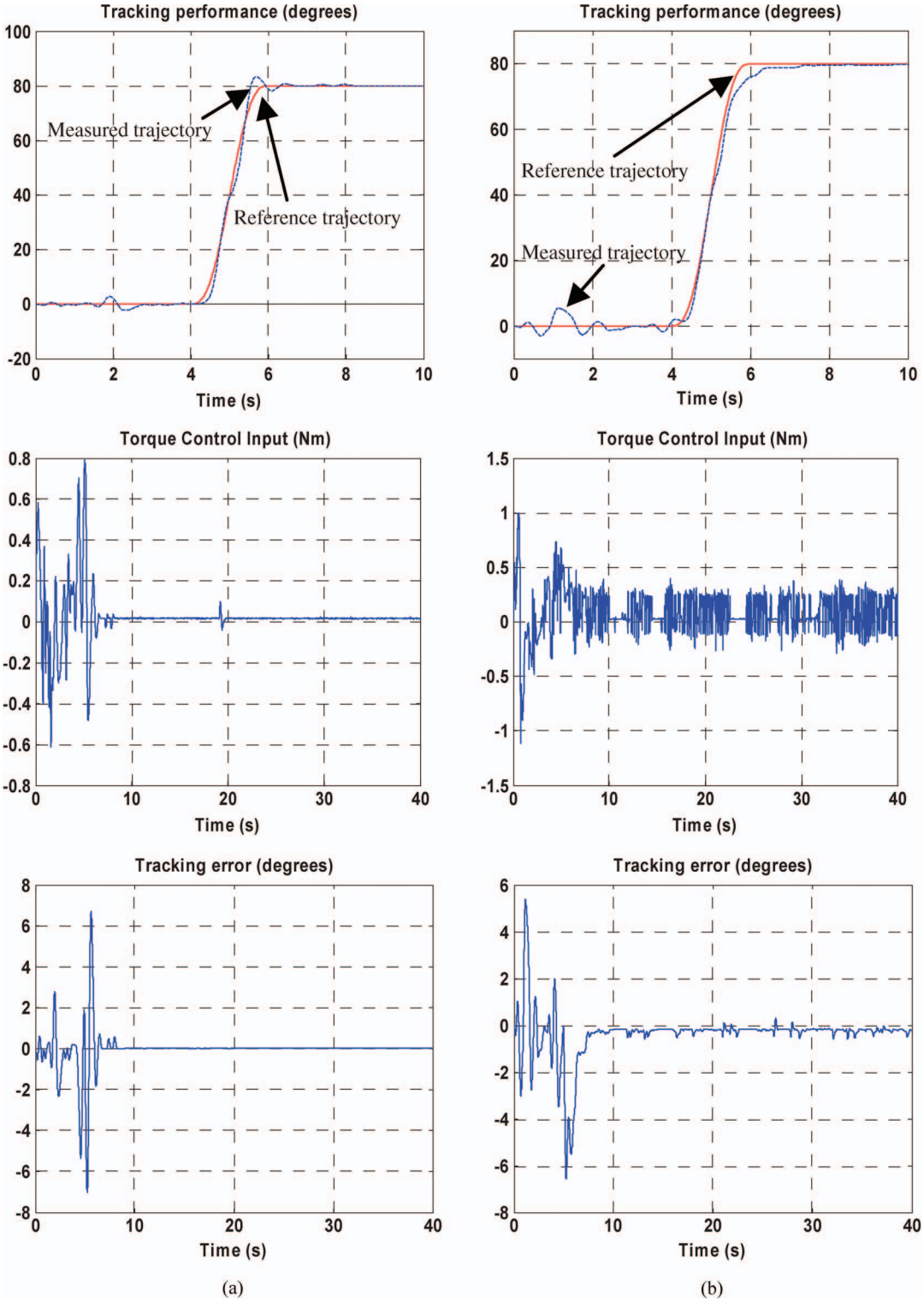

Fig. 6. Experimental results for joint 3 (a) with the reaching law and (b) with the conventional law. (a) ERL approach. (b) Conventional approach.

VII. Conclusion

In this paper, sliding-mode control has been experimentally applied to MIMO nonlinear systems. The main contribution of this paper is to introduce an ERL approach to the control mechanism in order to control both the chattering and tracking performances, which is impossible to achieve with the conventional sliding-mode control approach. Experimental results on a robot arm with 3 DOF showed the superiority of the proposed approach over the conventional control, particularly regarding the reduction of chattering levels on the control input.

APPENDIX
ROBOT'S PARAMETERS

1) Structure of $M(q,\dot{q})$ and $F(q,\dot{q})$:

$$\begin{aligned}
M(1,1) &= I_{zz1}+I_{zz2}+I_{zz3}+2m_3L^2c_{23}+2m_2L^2c_2\\
&\quad +2m_3L^2c_3+2m_3L^2c_2+m_1L^2+2m_2L^2\\
&\quad +3m_3L^2\\
M(2,1) &= I_{zz2}+I_{zz3}+2m_3L^2c_3+m_3L^2c_2+m_2L^2c_2\\
&\quad +m_3L^2c_{23}+2m_3L^2+m_2L^2\\
M(3,1) &= I_{zz3}+m_3L^2+m_3L^2c_3+m_3L^2c_{23},\\
M(1,2) &= M(2,1)\\
M(2,2) &= I_{zz2}+I_{zz3}+2m_3L^2+m_2L^2+2m_3L^2c_3\\
M(3,2) &= I_{zz3}+m_3L^2+m_3L^2c_3\\
M(1,3) &= M(3,1) \qquad M(2,3)=M(3,2),\\
M(3,3) &= I_{zz3}+m_3L^2\\
F(1) &= -L^2\left(m_3\dot{q}_2^2s_2+m_2\dot{q}_2^2s_2+m_3\dot{q}_3^2s_3+m_3\dot{q}_2^2s_{23}\right.\\
&\quad +m_3\dot{q}_3^2s_{23}+2m_3\dot{q}_3\dot{q}_1s_{23}+2m_2\dot{q}_1\dot{q}_2s_2\\
&\quad +2m_3\dot{q}_1\dot{q}_2s_2+2m_3\dot{q}_2\dot{q}_3s_3+2m_3\dot{q}_1\dot{q}_3s_3\\
&\quad \left.+2m_3\dot{q}_1\dot{q}_2s_{23}+2m_3\dot{q}_2\dot{q}_3s_{23}\right)\\
F(2) &= L^2\left(-2m_3\dot{q}_1\dot{q}_3s_3-m_3\dot{q}_3^2s_3-2m_3\dot{q}_3\dot{q}_2s_3\right.\\
&\quad \left.+m_3\dot{q}_1^2s_{23}+m_3\dot{q}_1^2s_2+m_2\dot{q}_1^2s_2\right)\\
F(3) &= m_3L^2\left(2\dot{q}_1\dot{q}_2s_3+\dot{q}_1^2s_{23}+\dot{q}_2^2s_3+\dot{q}_1^2s_3\right)
\end{aligned}$$

where $s_i=\sin(q_i)$, $c_i=\cos(q_i)$, $s_{ij}=\sin(q_i+q_j)$, and $c_{ij}=\cos(q_i+q_j)$.

2) Kinematic parameters:

$$L = 0.1228 \text{ m}.$$

3) Estimated dynamics parameters:

$$m_1=m_2=m_3=3 \text{ kg}$$
$$I_{zz1}=I_{zz2}=I_{zz3}=0.0038 \text{ kg}\cdot\text{m}^2.$$

4) Reference trajectory parameters:

$$\begin{aligned}
&q_{10}^d=q_{20}^d=q_{30}^d=0 && q_{1f}^d=80^\circ &&\\
&q_{2f}^d=-80^\circ && q_{3f}^d=80^\circ && t_{01}=0 \text{ s}\\
&t_{02}=2 \text{ s} && t_{03}=6 \text{ s} && t_1=2 \text{ s}.
\end{aligned}$$

5) Conventional reaching law parameters:

$$\lambda_1=\lambda_2=\lambda_3=10 \qquad k_1=k_2=k_3=10.$$

6) ERL parameters:

$$\begin{aligned}
&\lambda_1=\lambda_2=\lambda_3=10 && k_1=k_2=k_3=1\\
&\delta_{01}=\delta_{02}=\delta_{03}=0.1 &&\\
&\alpha_1=\alpha_2=\alpha_3=20 && p_1=p_2=p_3=1.
\end{aligned}$$

7) Sampling time: $T_s=0.0003$ s.

Proof of Relationship (20)

Using a symbolic software (MATHEMATICA)

$$\int_0^{|S(0)|} e^{-\alpha|S|^P}\,dS = \frac{\Gamma\left(1+\frac{1}{p}\right)-\frac{1}{p}\Gamma\left(\frac{1}{p},\alpha\,|S(0)|^p\right)}{\alpha^{1/p}}$$

where $\Gamma(a)$ is the Euler gamma function, and $\Gamma(a,z)$ is the incomplete gamma function defined as follows:

$$\Gamma(a)=\int_0^\infty t^{a-1}e^{-t}dt$$

$$\Gamma(a,z)=\int_z^\infty t^{a-1}e^{-t}dt \le \Gamma(a), \qquad z\ge 0.$$

It is straightforward that $(1/p)\cdot\Gamma(1/p,\alpha|S(0)|^p)\le(1/p)\cdot\Gamma(1/p)$.

On the other hand, using the properties of Γ, $(1/p)\Gamma(1/p)=\Gamma(1+(1/p))$, then $(1/p)\cdot\Gamma(1/p,\alpha|S(0)|^p)\le\Gamma(1+(1/p))$.

This is expected since $\int_0^{|S(0)|}e^{-\alpha|S|^P}dS$ is always positive. This implies that $\Gamma(1+(1/p))-(1/p)\Gamma(1/p,\alpha|S(0)|^p)\le\Gamma(1+(1/p))$.

From Γ's properties, $\Gamma(1+(1/p))\le 1$ for $p\ge 1$ with $\Gamma(1)=\Gamma(2)=1$; therefore, $\int_0^{|S(0)|}e^{-\alpha|S|^P}dS\le(1/\alpha^{1/p})$, and relation (20) is therefore straightforward.

REFERENCES

[1] A. Isidori, *Nonlinear Control Systems*. Berlin, Germany: Springer-Verlag, 1995.

[2] C.-W. Park and Y.-W. Cho, "Robust fuzzy feedback linearization controllers for Takagi–Sugeno fuzzy models with parametric uncertainties," *Control Theory Appl., IET*, vol. 1, no. 5, pp. 1242–1254, Sep. 2007.

[3] M. Krstic, I. Kanellakopoulos, and P. Kokotovic, *Nonlinear and Adaptive Control Design*. New York: Wiley, 1995.

[4] H.-J. Shieh and C.-H. Hsu, "An adaptive approximator-based backstepping control approach for piezoactuator-driven stages," *IEEE Trans. Ind. Electron.*, vol. 55, no. 4, pp. 1729–1738, Apr. 2008.

[5] M. Krstic, "Feedback linearizability and explicit integrator forwarding controllers for classes of feedforward systems," *IEEE Trans. Autom. Control*, vol. 49, no. 10, pp. 1668–1682, Oct. 2004.

[6] C.-M. Lin and C.-F. Hsu, "Recurrent-neural-network-based adaptive-backstepping control for induction servomotors," *IEEE Trans. Ind. Electron.*, vol. 52, no. 6, pp. 1677–1684, Dec. 2005.

[7] V. Utkin, *Sliding Mode in Control and Optimization*. Berlin, Germany: Springer-Verlag, 1992.

[8] R. A. Decarlo, S. H. Zak, and G. P. Matthews, "Variable structure control of nonlinear multivariable systems: A tutorial," *Proc. IEEE*, vol. 76, no. 3, pp. 212–232, Mar. 1988.

[9] B. Castillo-Toledo, S. Di Gennaro, A. G. Loukianov, and J. Rivera, "Hybrid control of induction motors via sampled closed representations," *IEEE Trans. Ind. Electron.*, vol. 55, no. 10, pp. 3758–3771, Oct. 2008.

[10] Y.-W. Liang, S.-D. Xu, D.-C. Liaw, and C.-C. Chen, "A study of T–S model-based SMC scheme with application to robot control," *IEEE Trans. Ind. Electron.*, vol. 55, no. 11, pp. 3964–3971, Nov. 2008.

[11] M. A. Fnaiech, F. Betin, G.-A. Capolino, and F. Fnaiech, "Fuzzy logic and sliding-mode controls applied to six-phase induction machine with open phases," *IEEE Trans. Ind. Electron.*, vol. 57, no. 1, pp. 354–364, Jan. 2010.

[12] T. Orlowska-Kowalska, M. Dybkowski, and K. Szabat, "Adaptive sliding-mode neuro-fuzzy control of the two-mass induction motor drive without mechanical sensors," *IEEE Trans. Ind. Electron.*, vol. 57, no. 2, pp. 553–564, Feb. 2010.

[13] L. Wang, T. Chai, and L. Zhai, "Neural-network-based terminal sliding-mode control of robotic manipulators including actuator dynamics," *IEEE Trans. Ind. Electron.*, vol. 56, no. 9, pp. 3296–3304, Sep. 2009.

[14] P. Pranayanuntana and V. Riewruja, "Nonlinear backstepping control design applied to magnetic ball control," *Proc. IEEE Intell. Syst. Technol. New Millennium*, pp. 304–307, 2000.
[15] T. Floquet, J. P. Barbot, and W. Perruquetti, "Higher order sliding mode stabilization for a class of nonholomic perturbed system," *Automatica*, vol. 39, no. 6, pp. 1077–1083, Jun. 2003.
[16] F. Hamerlain, K. Achour, T. Floquet, and W. Perruquetti, "Trajectory tracking of a car-like robot using second order sliding mode control," in *Proc. Eur. Control Conf.*, Kos, Greece, 2007.
[17] G. Bartolini, A. Ferrara, and E. Usai, "Chattering avoidance by second-order sliding mode control," *IEEE Trans. Autom. Control*, vol. 43, no. 2, pp. 241–246, Feb. 1998.
[18] G. Bartolini, A. Ferrara, E. Usai, and V. I. Utkin, "On multi-input chattering-free second-order sliding mode control," *IEEE Trans. Autom. Control*, vol. 49, no. 9, pp. 1711–1717, Sep. 2000.
[19] V. Parra-Vega and G. Hirzinger, "Chattering free sliding mode for a class of nonlinear mechanical systems," *Int. J. Robust Nonlinear Control*, vol. 11, no. 11, pp. 1161–1178, Oct. 2001.
[20] J. T. Moura and N. Olgac, "Robust Lyapunov control with perturbation estimation," *Proc. Inst. Elect. Eng.—Control Theory Appl.*, vol. 145, no. 3, pp. 307–315, May 1998.
[21] O. Camacho, R. Rojas, and W. García, "Variable structure control applied to a chemical processes with inverse response," *ISA Trans.*, vol. 38, no. 1, pp. 55–72, Jan. 1999.
[22] W. Gao and J. C. Hung, "Variable structure control of nonlinear systems: A new approach," *IEEE Trans. Ind. Electron.*, vol. 40, no. 1, pp. 45–55, Feb. 1993.
[23] J. J. Slotine and W. Li, *Applied Nonlinear Control*. Englewood Cliffs, NJ: Prentice-Hall, 1991.
[24] M. Saad, P. Bigras, L. A. Dessaint, and K. Al-Haddad, "Adaptive robot control using neural networks," *IEEE Trans. Ind. Electron.*, vol. 41, no. 2, pp. 173–181, Apr. 1994.

Charles J. Fallaha was born in Beirut, Lebanon, in 1981. He received the Diploma degree in electromechanical engineering from the École Supérieure d'Ingénieurs of Beirut, Saint-Joseph University, Beirut, in 2004 and the M.S. degree in electrical engineering from the Ecole de Technologie Supérieure, Montreal, QC, Canada, in 2006.

He is currently an Aeronautical Engineer with CAE. His main research interests include linear/nonlinear and intelligent control, robotics, and power electronics.

Maarouf Saad (SM'97) received the B.S. and M.S. degrees in electrical engineering from Ecole Polytechnique of Montreal, Montreal, QC, Canada, in 1982 and 1984, respectively, and the Ph.D. degree in electrical engineering from McGill University, Montreal, in 1988.

In 1987, he joined Ecole de Technologie Supérieure, Montreal, where he is currently teaching control theory and robotics courses. His research is mainly in nonlinear control and optimization applied to robotics and flight control system.

Hadi Youssef Kanaan (S'99–M'02–SM'06) was born in Beirut, Lebanon, in 1967. He received the Diploma degree in electromechanical engineering from the Ecole Supérieure d'Ingénieurs of Beirut (ESIB), Saint-Joseph University, Beirut, in 1991 and the Ph.D. degree in electrical engineering from the Ecole de Technologie Supérieure, Montreal, QC, Canada, in 2002.

He is currently an Associate Professor with ESIB, Saint-Joseph University, where he was an Assistant Teacher between 1992 and 1995, an Invited Professor in 1997–2001, and an Assistant Professor in 2001–2009. His research interests concern the modeling and control of switch-mode converters, modern rectifiers, power factor correction, active power filters, fault detection and monitoring of drive systems, intelligent control, neural networks, and fuzzy logic. He has published more than 100 papers in international journals and conferences.

Dr. Kanaan is currently an Associate Editor of the IEEE TRANSACTIONS ON INDUSTRIAL ELECTRONICS, the Treasurer of the Power and Energy/Power Electronics/Circuits and Systems joint Chapter of the IEEE Lebanon Section, and a Counselor of the IEEE Student Branch in ESIB.

Kamal Al-Haddad (S'82–M'88–SM'92–F'07) was born in Beirut, Lebanon, in 1954. He received the B.Sc.A. and M.Sc.A. degrees from the Université du Québec à Trois-Rivières, Trois-Rivières, QC, Canada, in 1982 and 1984, respectively, and the Ph.D. degree from the Institut National Polytechnique, Toulouse, France, in 1988.

From June 1987 to June 1990, he was a Professor with the Engineering Department, Université du Québec à Trois-Rivières. Since June 1990, he has been a Professor with the Department of Electrical Engineering, École de Technologie Supérieure, Montreal, QC. His fields of interest are static power converters, harmonics and reactive power control, and switch mode and resonant converters, including the modeling, control, and development of industrial prototypes for various applications.

Dr. Al-Haddad is a member of the Order of Engineering of Quebec and the Canadian Institute of Engineers. He is also the holder of Canada Research Chair in Energy Conversion and Power Electronics.